

LINEAR AND NONLINEAR PARAREAL METHODS FOR THE CAHN-HILLIARD EQUATION

GOBINDA GARAI, BANKIM C. MANDAL

ABSTRACT. In this paper, we propose, analyze and implement efficient time parallel methods for the Cahn-Hilliard (CH) equation. It is of great importance to develop efficient numerical methods for the CH equation, given the range of applicability of the CH equation has. The CH equation generally needs to be simulated for a very long time to get the solution of phase coarsening stage. Therefore it is desirable to accelerate the computation using parallel method in time. We present linear and nonlinear Parareal methods for the CH equation depending on the choice of fine approximation. We illustrate our results by numerical experiments.

1. INTRODUCTION

We are interested in designing time parallel algorithms for the Cahn-Hilliard equation

$$\begin{cases} \frac{\partial u}{\partial t} + \epsilon^2 \Delta^2 u = \Delta f(u), & (x, t) \in \Omega \times (0, T], \\ u = 0 = \partial_\nu(\nabla u), & (x, t) \in \partial\Omega \times (0, T], \\ u(x, 0) = u^0, & x \in \Omega, \end{cases} \quad (1.1)$$

where ν is the outward unit normal to $\partial\Omega$. The CH equation has been suggested as a prototype to represent the evolution of a binary melted alloy below the critical temperature in [4, 5]. The CH equation (1.1) also arises from the Ginzburg-Landau energy functional:

$$\mathcal{E}(u) := \int_{\Omega} \left(F(u) + \frac{\epsilon^2}{2} |\nabla u|^2 \right) dx, \quad (1.2)$$

by considering (1.1) as a gradient flow $\frac{\partial u}{\partial t} = \Delta \frac{\delta \mathcal{E}}{\delta u}$, where $\frac{\delta \mathcal{E}}{\delta u}$ is the first variation of energy, $F(u) = 0.25(u^2 - 1)^2$ with $F'(u) = f(u)$, and $\epsilon(0 < \epsilon \ll 1)$ is the thickness of the interface. The solution of (1.1) involves two different dynamics, one is phase separation which is quick in time, and another is phase coarsening which is slow in time. The fine-scale phase regions are formed during the early stage of the dynamics of width ϵ . Whereas during the phase coarsening stage, the solution tends to an equilibrium state which minimizes the system energy in (1.2). By differentiating the energy functional $\mathcal{E}(u)$ and total mass $\int_{\Omega} u$ with respect to time t , we get

$$\frac{d}{dt} \mathcal{E}(u) \leq 0, \quad \frac{d}{dt} \int_{\Omega} u = 0. \quad (1.3)$$

2020 *Mathematics Subject Classification.* 65M12, 65Y05, 65M15, 65Y20.

Key words and phrases. Parallel-in-Time (PinT), Parallel computing, Convergence analysis, Cahn-Hilliard equation, Parareal method.

Submitted.

So the CH equation describes energy minimization and the total mass conservation while the system evolves.

The existence of the solution of the CH equation (1.1) can be seen from [7] and also results for other variants of the CH equation are shown in [9, 22]. Various research have been done in finding numerical scheme for the CH equation to approximate the solution with either Dirichlet [7, 10] or Neumann boundary conditions [8, 14, 26, 24] and references therein. Recently a new approach to approximate the solution of the CH equation has been proposed in [28, 29] based on quadratization of the energy $\mathcal{E}(u)$ of the CH equation. A modification on energy quadratization approach yields a new method known as scalar auxiliary variable [23]. A review on numerical treatment of the CH equation can be found in [20]. The possible application of CH equation as a model are: image inpainting [2], tumour growth simulation [27], population dynamics [6], dendritic growth [19], planet formation [25], etc.

The above described works are all in time stepping fashion for advancement of evolution of the CH equation. Therefore to get a solution of CH equation need to be solved sequentially over long time for capturing the long term behaviour of the CH equation, specially the phase coarsening stage. Consequently, it is of great importance to accelerate the simulation using parallel computation, which can be fulfilled by time parallel techniques. In last few decades there is a lot of efforts on formulating various type of time parallel techniques, for an overview see [15]. To speed-up the computation we construct the Parareal methods for the CH equation (1.1). The Parareal method [21] is a well known iterative time parallel method, that can also be viewed as multiple shooting method or time-multigrid method; see [16]. The method rely on computing fine and coarse resolution and eventually converge to fine resolution. It has been successfully applied to: fluid-structure interaction in [12], Navier-Stokes equation in [13], molecular-dynamics in [1]. The main objective of this work is to adapt the Parareal algorithm for the CH equation (1.1) and study the convergence behaviour.

The rest of this paper is arranged as follows. We introduce in Section 2 the time parallel algorithm for equation (1.1). In section 3 we present the stability and convergence results. To illustrate our analysis, the accuracy and robustness of the proposed formulation, we show numerical results in Section 4.

2. PARAREAL METHOD

To solve the following system of ODEs

$$\frac{du}{dt} = f(t, u), \quad u(0) = u^0, \quad t \in (0, T], \quad (2.1)$$

Lions et al. proposed the Parareal algorithm in [21], where $f : \mathbb{R}^+ \times \mathbb{R}^d \rightarrow \mathbb{R}^d$ is Lipschitz. The method constitutes of the following strategy: first a non-overlapping decomposition of time domain $(0, T]$ into N smaller subintervals of uniform size, i.e., $(0, T] = \cup_{n=1}^N [T_{n-1}, T_n]$ with $T_n - T_{n-1} = \Delta T = T/N$ is considered, secondly each time slice $[T_{n-1}, T_n]$ is divided into J smaller time slices with $\Delta t = \Delta T/J$, then a fine propagator \mathcal{F} which is expensive but accurate, and a coarse propagator \mathcal{G} which is cheap but may be inaccurate are assigned to compute the solution in fine grid and coarse grid respectively. Then the Parareal algorithm for (2.1) starts with the initial approximation U_n^0 at T_n 's, obtained by the coarse operator \mathcal{G} and

solve the following prediction-correction scheme for $k = 0, 1, \dots$

$$\begin{aligned} U_0^{k+1} &= u^0, \\ U_{n+1}^{k+1} &= \mathcal{G}(T_{n+1}, T_n, U_n^{k+1}) + \mathcal{F}(T_{n+1}, T_n, U_n^k) - \mathcal{G}(T_{n+1}, T_n, U_n^k), \end{aligned} \quad (2.2)$$

where operator $\mathcal{S}(T_{n+1}, T_n, U_n^k)$ provides solution at T_{n+1} by taking the initial solution U_n^k at T_n for $\mathcal{S} = \mathcal{F}$ or \mathcal{G} . At current iteration U_n^k 's are known, hence one computes $\mathcal{F}(T_{n+1}, T_n, U_n^k)$ in parallel using N processor. The Parareal solution converges towards the fine resolution in finite steps. To get a practical parallel algorithm we should have $k \ll N$.

2.1. Discretization and Formulation. To formulate the Parareal method for the CH equation (1.1) we first look into possible discretization of (1.1) in both spatial and temporal variables. Since the non-increasing of the total energy and mass conservation property (1.3) are essential features of the CH equation (1.1), they are expected to be preserved for long time simulation under any proposed numerical scheme as well. To deal with this, Eyre proposed an unconditionally gradient stable scheme in [10, 11]. The idea is to split the homogeneous free energy

$$F(u) = \underbrace{\frac{u^4}{4}}_{\text{convex part}} + \underbrace{\frac{-u^2}{2}}_{\text{concave part}} \quad \text{into a sum of a convex and a concave term, and}$$

then treat the convex term implicitly and the concave term explicitly to obtain a nonlinear approximation for (1.1) in 1D as:

$$u_j^{n+1} - u_j^n = \Delta t D_h (u_j^{n+1})^3 - \Delta t D_h u_j^n - \epsilon^2 \Delta t D_h^2 u_j^{n+1}, \quad (2.3)$$

where Δt is the time step and D_h is the discrete Laplacian and the scheme is $O(\Delta t) + O(\Delta x^2)$ accurate [10, 11]. The scheme (2.3) is unconditionally gradient stable, means the discrete energy is non-increasing for every time step Δt . To get a linear approximation of (1.1), the term $(u_j^{n+1})^3$ in (2.3) is rewritten as $(u_j^n)^2 u_j^{n+1}$, which leads to the following linear approximation

$$u_j^{n+1} - u_j^n = \Delta t D_h (u_j^n)^2 u_j^{n+1} - \Delta t D_h u_j^n - \epsilon^2 \Delta t D_h^2 u_j^{n+1}. \quad (2.4)$$

This is also an unconditionally gradient stable scheme and has the same accuracy as the previous nonlinear scheme (2.3) [10]. Another convex-concave splitting of $F(u)$

$$\text{is } F(u) = \underbrace{u^2 + \frac{1}{4}}_{\text{convex part}} + \underbrace{\frac{u^4}{4} - \frac{3u^2}{2}}_{\text{concave part}}, \text{ and by treating the convex part implicitly and}$$

concave part explicitly one obtains the following unconditionally gradient stable linear scheme [11]

$$u_j^{n+1} - u_j^n = \Delta t D_h (u_j^n)^3 - 3\Delta t D_h u_j^n - \epsilon^2 \Delta t D_h^2 u_j^{n+1} + 2\Delta t u_j^{n+1}. \quad (2.5)$$

Now to employ the discrete Parareal method for the CH equation (1.1) we denote U_n^k as the approximation at k -th iteration containing $u(jh, T_n)$, $j = 2, 3, \dots, N_x - 1$, where h is the spatial mesh size and N_x is the number of discrete nodes in spatial domain. Now depending on the choice of coarse and fine operator we propose the following five versions of Parareal algorithms for the CH equation (1.1):

- (1) We fix both the fine propagator \mathcal{F} and coarse propagator \mathcal{G} to be the linear scheme in (2.4) in the Parareal iteration (2.2). We call this algorithm PA-I.

- (2) We fix both the fine propagator \mathcal{F} and coarse propagator \mathcal{G} to be the linear scheme in (2.5) in the Parareal iteration (2.2). We call this algorithm PA-II.
- (3) We fix the fine propagator \mathcal{F} to be the linear scheme in (2.5) and coarse propagator \mathcal{G} to be the linear scheme in (2.4) in the Parareal iteration (2.2). We call this algorithm PA-III.
- (4) We fix the fine propagator \mathcal{F} to be the nonlinear scheme in (2.3) and coarse propagator \mathcal{G} to be the linear scheme in (2.4) in the Parareal iteration (2.2). We call this algorithm NPA-I.
- (5) We fix both the fine propagator \mathcal{F} and coarse propagator \mathcal{G} to be the nonlinear scheme in (2.3) in the Parareal iteration (2.2). We call this algorithm NPA-II.

The first three algorithms are linear whereas the last two algorithms are nonlinear as either the fine solver or the coarse solver or both involve nonlinear scheme. Next we discuss the stability and convergence properties of the proposed Parareal algorithms.

3. STABILITY AND CONVERGENCE

First we rewrite the fine and coarse propagators in simplified operator form. For the approximation in (2.4) we have

$$\frac{W^{n+1} - W^n}{\Delta t} = D_h \operatorname{diag}(W^n)^2 W^{n+1} - \epsilon^2 D_h^2 W^{n+1} - D_h W^n, \quad (3.1)$$

where $W \in \mathbb{R}^{(N_x-2)}$ and the discrete Laplacian D_h with Dirichlet boundary condition is the following

$$D_h = \frac{1}{h^2} \begin{bmatrix} -2 & 1 & & & \\ 1 & -2 & 1 & & \\ & \ddots & \ddots & \ddots & \\ & & 1 & -2 & 1 \\ & & & 1 & -2 \end{bmatrix} \in \mathbb{R}^{(N_x-2) \times (N_x-2)}. \quad (3.2)$$

Numerical tests suggest that the term $\operatorname{diag}(W^n)^2$ behaves as I , away from interface region, which also observed in [10]. Thus for analysing purpose we consider $\operatorname{diag}(W^n)^2 \approx I$. Then (3.1) can be written as $W^{n+1} = (I - \Delta t D_h + \epsilon^2 \Delta t D_h^2)^{-1} (I - \Delta t D_h) W^n$, where I is the identity matrix. Then the fine and coarse propagator corresponding to the scheme (2.4) can be written as

$$\mathcal{F}(T_{n+1}, T_n, U) = (I - \Delta t D_h + \epsilon^2 \Delta t D_h^2)^{-1} (I - \Delta t D_h) U, \quad U \in \mathbb{R}^{N_x-2}, \quad (3.3a)$$

$$\mathcal{G}(T_{n+1}, T_n, U) = (I - \Delta t D_h + \epsilon^2 \Delta t D_h^2)^{-1} (I - \Delta t D_h) U, \quad U \in \mathbb{R}^{N_x-2}, \quad (3.3b)$$

respectively. Similarly we can write the fine and coarse propagator corresponding to the scheme (2.5) as

$$\mathcal{F}(T_{n+1}, T_n, U) = (I - 2\Delta t D_h + \epsilon^2 \Delta t D_h^2)^{-1} (I - 2\Delta t D_h) U, \quad U \in \mathbb{R}^{N_x-2}, \quad (3.4a)$$

$$\mathcal{G}(T_{n+1}, T_n, U) = (I - 2\Delta t D_h + \epsilon^2 \Delta t D_h^2)^{-1} (I - 2\Delta t D_h) U, \quad U \in \mathbb{R}^{N_x-2}. \quad (3.4b)$$

The matrix D_h in (3.2) is symmetric negative definite; eigenvalues of D_h are $\lambda_p = \frac{2}{h^2} \left\{ \cos \left(\frac{p\pi}{N_x-1} \right) - 1 \right\}, p = 1, \dots, N_x - 2$. λ_p 's are distinct and satisfy $\lambda_p <$

$0, \forall p$. Now we define few matrices that we use later in the paper. The matrices are $P_i := (I - i\Delta T D_h + \epsilon^2 \Delta T D_h^2)^{-1} (I - i\Delta T D_h)$ for $i = 1, 2, 3$ and $P_{J_i} := \left[(I - \frac{i\Delta T}{J} D_h + \epsilon^2 \frac{\Delta T}{J} D_h^2)^{-1} (I - \frac{i\Delta T}{J} D_h) \right]^J$ for $i = 1, 2$. Before stating the stability and convergence results for the linear Parareal algorithms we first state and prove some auxiliary results.

Lemma 3.1. *Let $J \in \mathbb{N}$ such that $J \geq 2, \Delta T > 0, \epsilon > 0$ and $y \in (0, \infty)$. Then the functions $g_i(y) = \frac{1+i\Delta T y}{1+i\Delta T y + \epsilon^2 \Delta T y^2}$ for $i = 1, 2, 3$ satisfy $g_i(y) \in (0, 1), \forall y$.*

Proof. It is clear that each g_i is continuous in $(0, \infty)$, and $\lim_{y \rightarrow 0^+} g_i(y) = 1$ and $\lim_{y \rightarrow \infty} g_i(y) = 0$, so we have $g_i(y) \in (0, 1), \forall y$. \square

Lemma 3.2. *Let $J \in \mathbb{N}$ such that $J \geq 2, \Delta T > 0, \epsilon > 0$ and $y \in (0, \infty)$. Then the followings hold*

(i) *for $i = 1, 2$ the function $\phi_i(y) := (g_i(y/J))^J - g_i(y)$ satisfies $|\phi_i(y)| < 1, \forall y$.*

(ii) *the function $\phi_3(y) := (g_2(y/J))^J - g_1(y)$ satisfies $|\phi_3(y)| < 1, \forall y$.*

Proof. First we prove the statement (i). We have $|\phi_i(y)| < 1 \iff (g_i(y/J))^J < 1 + g_i(y) \& (g_i(y/J))^J > -1 + g_i(y)$. Using Lemma 3.1 we have $g_i^J(y/J) \in (0, 1)$ and thus we have $g_i^J(y/J) < 1 + g_i(y), \forall y$. The term $-1 + g_i(y) = \frac{-\epsilon^2 \Delta T y^2}{1+i\Delta T y + \epsilon^2 \Delta T y^2} < 0$, hence $(g_i(y/J))^J > -1 + g_i(y)$ holds. Similarly we can get the result (ii). \square

Lemma 3.3 (Matrix inverse). *Let $n \in \mathbb{N}, \beta \in \mathbb{R}^+$ then*

$$M(\beta)^{-1} := \begin{bmatrix} 1 & 0 & & & \\ -\beta & 1 & 0 & & \\ & \ddots & \ddots & \ddots & \\ & & -\beta & 1 & 0 \\ & & & -\beta & 1 \end{bmatrix}_{n \times n}^{-1} = \begin{bmatrix} 1 & 0 & & & \\ \beta & 1 & 0 & & \\ \vdots & & \ddots & \ddots & \\ \beta^{n-2} & \beta^{n-3} & \dots & 1 & 0 \\ \beta^{n-1} & \beta^{n-2} & \dots & \beta & 1 \end{bmatrix}_{n \times n} \quad (3.5)$$

Proof. We prove the result (3.5) by induction. Clearly the statement is true for $n = 2$. Let us assume that the result (3.5) is true for $n = l$. Then for $n = l + 1$ the matrix $M(\beta)$ can be written as the following block form

$$M(\beta) = \begin{bmatrix} A_{l \times l} & B_{l \times 1} \\ C_{1 \times l} & D_{1 \times 1} \end{bmatrix}_{(l+1) \times (l+1)}, \quad (3.6)$$

where $A = M(\beta)_{l \times l}, B = [\mathbf{0}]_{l \times 1}, C = [\mathbf{0}, -\beta]_{1 \times l}, D = [1]_{1 \times 1}$. As we know the inverse of A we have

$$M(\beta)^{-1}_{(l+1) \times (l+1)} = \begin{bmatrix} A^{-1} + A^{-1} B S^{-1} C A^{-1} & -A^{-1} B S^{-1} \\ -S^{-1} C A^{-1} & S^{-1} \end{bmatrix}, \quad (3.7)$$

where $S = D - C A^{-1} B$. Clearly $S^{-1} = [1]_{1 \times 1}$, and thus we have $A^{-1} B S^{-1} C A^{-1} = [\mathbf{0}]_{l \times l}, -A^{-1} B S^{-1} = [\mathbf{0}]_{l \times 1}$, and $-S^{-1} C A^{-1} = [\beta^l, \beta^{l-1}, \dots, \beta]_{1 \times l}$. Hence we have the Lemma. \square

Lemma 3.4 (Matrix power). *Let $\beta > 0$ and $\mathbb{T}(\beta)$ be a strictly lower triangular Toeplitz matrix of size N whose elements are defined by its first column*

$$\mathbb{T}_{i,1} = \begin{cases} 0 & \text{if } i = 1, \\ \beta^{i-2} & \text{if } 2 \leq i \leq N. \end{cases}$$

Then the i -th element of the first column of the k -th power of \mathbb{T} is

$$\mathbb{T}_{i,1}^k = \begin{cases} 0 & \text{if } 1 \leq i \leq k, \\ \binom{i-2}{k-1} \beta^{i-1-k} & \text{if } k+1 \leq i \leq N. \end{cases}$$

Proof. See [16]. □

Lemma 3.5. *For $0 < \beta < 1$ the infinity norm of $\mathbb{T}(\beta)^k$ is given by*

$$\|\mathbb{T}^k\|_\infty \leq \min \left\{ \left(\frac{1-\beta^{N-1}}{1-\beta} \right)^k, \binom{N-1}{k} \right\}$$

Proof. See [16]. □

Theorem 3.6 (Stability of PA-I). *The algorithm PA-I is stable, i.e., for each n and k the Parareal iteration satisfies $\|U_{n+1}^{k+1}\| \leq \|u^0\| + (n+1) \left(\max_{0 \leq j \leq n} \|U_j^k\| \right)$.*

Proof. Using the fine propagator (3.3a) and coarse propagator (3.3b) in the Parareal scheme (2.2) we have

$$\begin{aligned} U_{n+1}^{k+1} &= P_1 U_n^{k+1} + (P_{J_1} - P_1) U_n^k, \\ \xrightarrow{\text{by taking norm}} \|U_{n+1}^{k+1}\| &\leq \|P_1\| \|U_n^{k+1}\| + \|P_{J_1} - P_1\| \|U_n^k\| \\ &\leq \|U_n^{k+1}\| + \|U_n^k\|, \end{aligned} \tag{3.8}$$

where in the second inequality (3.8) we use Lemma 3.1 & 3.2. By the repeated application of the recurrence in (3.8) for n and taking the sum we have

$$\|U_{n+1}^{k+1}\| - \|U_0^{k+1}\| \leq \sum_{j=0}^n \|U_j^k\| \leq (n+1) \left(\max_{0 \leq j \leq n} \|U_j^k\| \right).$$

Then using $U_0^{k+1} = u^0$ we get the stated result. □

Theorem 3.7 (Convergence of PA-I). *The algorithm PA-I is convergent, i.e., for the error $E_{n+1}^{k+1} = U(T_{n+1}) - U_{n+1}^{k+1}$ the algorithm PA-I satisfies the following error estimate $\max_{1 \leq j \leq N} \|E_j^{k+1}\| \leq \alpha^{k+1} \min \left\{ \left(\frac{1-\beta^{N-1}}{1-\beta} \right)^{k+1}, \binom{N-1}{k+1} \right\} \max_{1 \leq j \leq N} \|E_j^0\|$, where $\alpha = \|P_{J_1} - P_1\|, \beta = \|P_1\|$.*

Proof. From the Parareal scheme (2.2) we have

$$\begin{aligned} U(T_{n+1}) - U_{n+1}^{k+1} &= U(T_{n+1}) - \mathcal{G}(T_{n+1}, T_n, U_n^{k+1}) - \mathcal{F}(T_{n+1}, T_n, U_n^k) + \mathcal{G}(T_{n+1}, T_n, U_n^k) \\ &= \mathcal{F}(T_{n+1}, T_n, U_n) - \mathcal{G}(T_{n+1}, T_n, U_n) \\ &\quad - (\mathcal{F}(T_{n+1}, T_n, U_n^k) - \mathcal{G}(T_{n+1}, T_n, U_n^k)) \\ &\quad + \mathcal{G}(T_{n+1}, T_n, U_n) - \mathcal{G}(T_{n+1}, T_n, U_n^{k+1}). \end{aligned} \tag{3.9}$$

Using the fine propagator (3.3a) and coarse propagator (3.3b) in (3.9) we have the recurrence relation for the error E_{n+1}^{k+1} as

$$E_{n+1}^{k+1} = (P_{J_1} - P_1) E_n^k + P_1 E_n^{k+1},$$

$\xrightarrow{\text{by taking norm}} \|E_{n+1}^{k+1}\| \leq \|P_{J_1} - P_1\| \|E_n^k\| + \|P_1\| \|E_n^{k+1}\|.$ (3.10)

The recurrence relation in (3.10) can be written in the following matrix form

$$\begin{bmatrix} \|E_1\| \\ \|E_2\| \\ \vdots \\ \|E_{N-1}\| \\ \|E_N\| \end{bmatrix}^{k+1} \leq \begin{bmatrix} 1 & 0 & & & \\ -\beta & 1 & 0 & & \\ & \ddots & \ddots & \ddots & \\ & & -\beta & 1 & 0 \\ & & & -\beta & 1 \end{bmatrix}^{-1} \begin{bmatrix} 0 & 0 & & & \\ \alpha & 0 & 0 & & \\ & \ddots & \ddots & \ddots & \\ & & \alpha & 0 & 0 \\ & & & \alpha & 0 \end{bmatrix} \begin{bmatrix} \|E_1\| \\ \|E_2\| \\ \vdots \\ \|E_{N-1}\| \\ \|E_N\| \end{bmatrix}^k$$

$$\leq \alpha \begin{bmatrix} 0 & 0 & & & \\ 1 & 0 & 0 & & \\ \vdots & & \ddots & \ddots & \\ \beta^{N-3} & \beta^{N-4} & \cdots & 0 & 0 \\ \beta^{N-2} & \beta^{N-3} & \cdots & 1 & 0 \end{bmatrix} \begin{bmatrix} \|E_1\| \\ \|E_2\| \\ \vdots \\ \|E_{N-1}\| \\ \|E_N\| \end{bmatrix}^k,$$
 (3.11)

where $\alpha = \|P_{J_1} - P_1\|$, $\beta = \|P_1\|$, and on second inequality we use the Lemma 3.3. Now observe that the iteration matrix appearing in (3.11) is Nilpotent, so for $k = N$ we have finite step convergence. Using Lemma 3.4 and Lemma 3.5 in (3.11) we get the stated error contraction relation. \square

Theorem 3.8 (Stability of PA-II). *The algorithm PA-II is stable, i.e., for each n and k the Parareal iteration satisfies $\|U_{n+1}^{k+1}\| \leq \|u^0\| + (n+1) \left(\max_{0 \leq j \leq n} \|U_j^k\| \right)$.*

Proof. Emulating the proof of Theorem 3.6 we have the stated result. \square

Theorem 3.9 (Convergence of PA-II). *The algorithm PA-II is convergent, i.e., for the error $E_{n+1}^{k+1} = U(T_{n+1}) - U_{n+1}^{k+1}$ the algorithm PA-II satisfies the following error estimate $\max_{1 \leq j \leq N} \|E_j^{k+1}\| \leq \alpha^{k+1} \min \left\{ \left(\frac{1-\beta^{N-1}}{1-\beta} \right)^{k+1}, \binom{N-1}{k+1} \right\} \max_{1 \leq j \leq N} \|E_j^0\|$, where $\alpha = \|P_{J_2} - P_2\|$, $\beta = \|P_2\|$.*

Proof. The proof follows from the Theorem 3.7. \square

Theorem 3.10 (Stability of PA-III). *The algorithm PA-III is stable, i.e., for each n and k the Parareal iteration satisfies $\|U_{n+1}^{k+1}\| \leq \|u^0\| + (n+1) \left(\max_{0 \leq j \leq n} \|U_j^k\| \right)$.*

Proof. Emulating the proof of Theorem 3.6 we have the result. \square

Theorem 3.11 (Convergence of PA-III). *The algorithm PA-III is convergent, i.e., for the error $E_{n+1}^{k+1} = U(T_{n+1}) - U_{n+1}^{k+1}$ the algorithm PA-III satisfies the following error estimation $\max_{1 \leq j \leq N} \|E_j^{k+1}\| \leq \alpha^{k+1} \min \left\{ \left(\frac{1-\beta^{N-1}}{1-\beta} \right)^{k+1}, \binom{N-1}{k+1} \right\} \max_{1 \leq j \leq N} \|E_j^0\|$, where $\alpha = \|P_{J_2} - P_1\|$, $\beta = \|P_1\|$.*

Proof. The proof follows from the Theorem 3.7. \square

Next we prove a few relevant results before discussing the stability and convergence of nonlinear Parareal method.

Lemma 3.12 (Growth of Coarse Operator in NPA-I). *The coarse operator in (3.3b) satisfies the growth condition $\|\mathcal{G}(T_{n+1}, T_n, U)\| \leq \|U\|, \forall U \in \mathbb{R}^{N_x-2}$.*

Proof. We have $\|\mathcal{G}(T_{n+1}, T_n, U)\| \leq \|P_1\| \|U\|$. Now $\|P_1\| < 1$ follows from Lemma 3.1, hence the result. \square

Lemma 3.13 (Lipschitz Property of \mathcal{G}). *The coarse operator in (3.3b) satisfies the Lipschitz condition $\|\mathcal{G}(T_{n+1}, T_n, U_1) - \mathcal{G}(T_{n+1}, T_n, U_2)\| \leq \|P_1\| \|U_1 - U_2\|, \forall U_1, U_2 \in \mathbb{R}^{N_x-2}$.*

Proof. The result is straight forward. \square

Lemma 3.14 (Local Truncation Error (LTE) Differences in NPA-I). *Let $\mathcal{F}(T_{n+1}, T_n, U)$ be the fine operator generated by the nonlinear scheme in (2.3) and $\mathcal{G}(T_{n+1}, T_n, U)$ be the coarse operator in (3.3b). Then the following LTE differences hold*

$$\mathcal{F}(T_{n+1}, T_n, U) - \mathcal{G}(T_{n+1}, T_n, U) = c_2(U)\Delta T^2 + c_3(U)\Delta T^3 + \dots,$$

where $c_j(U)$ are continuously differentiable function for $j = 2, 3, \dots$

Proof. Let $\mathcal{S}(T_{n+1}, T_n, U)$ be the exact solution of (1.1), then

$$\begin{aligned} \mathcal{F}(T_{n+1}, T_n, U) - \mathcal{G}(T_{n+1}, T_n, U) &= \mathcal{F}(T_{n+1}, T_n, U) - \mathcal{S}(T_{n+1}, T_n, U) \\ &\quad + \mathcal{S}(T_{n+1}, T_n, U) - \mathcal{G}(T_{n+1}, T_n, U) \\ &= \tilde{c}_2(U)\Delta T^2 + \tilde{c}_3(U)\Delta T^3 + \dots \\ &\quad + \hat{c}_2(U)\Delta T^2 + \hat{c}_3(U)\Delta T^3 + \dots \\ &= c_2(U)\Delta T^2 + c_3(U)\Delta T^3 + \dots. \end{aligned}$$

Hence the Lemma. \square

Theorem 3.15 (Stability of NPA-I). *The algorithm NPA-I is stable, i.e., for each n and k , $\|U_{n+1}^{k+1}\| \leq \|u^0\| + C(n+1)\Delta T^2 \left(\max_{0 \leq j \leq n} \|U_j^k\| \right)$, for a constant C .*

Proof. Taking the norm in the correction scheme (2.2) we have

$$\begin{aligned} \|U_{n+1}^{k+1}\| &\leq \|\mathcal{G}(T_{n+1}, T_n, U_n^{k+1})\| + \|\mathcal{F}(T_{n+1}, T_n, U_n^k) - \mathcal{G}(T_{n+1}, T_n, U_n^k)\| \\ &\leq \|U_n^{k+1}\| + C\Delta T^2 \|U_n^k\|, \end{aligned} \quad (3.12)$$

where in the 2nd inequality we use Lemma (3.12) and (3.14). Takin the sum over n on the recurrence relation (3.12) we get

$$\|U_{n+1}^{k+1}\| - \|U_0^{k+1}\| \leq C\Delta T^2 \sum_{j=0}^n \|U_j^k\| \leq C(n+1)\Delta T^2 \left(\max_{0 \leq j \leq n} \|U_j^k\| \right).$$

Then using $U_0^{k+1} = u^0$ we get the stated result. \square

Theorem 3.16 (Convergence of NPA-I). *If the propagator \mathcal{F} in (2.3) and \mathcal{G} in (2.4) satisfy LTE differences given in Lemma 3.14 and \mathcal{G} satisfy Lipschitz condition given in Lemma 3.13, then the algorithm NPA-I satisfies the following error estimate*

$$\max_{1 \leq j \leq N} \|E_j^{k+1}\| \leq (C_1 \Delta T^2)^{k+1} \min \left\{ \left(\frac{1 - \beta^{N-1}}{1 - \beta} \right)^{k+1}, \binom{N-1}{k+1} \right\} \max_{1 \leq j \leq N} \|E_j^0\|,$$

where $\beta = \| P_1 \|$, and C_1 is a constant related to LTE.

Proof. From the Parareal scheme (2.2) we have

$$\begin{aligned}
U(T_{n+1}) - U_{n+1}^{k+1} &= U(T_{n+1}) - \mathcal{G}(T_{n+1}, T_n, U_n^{k+1}) - \mathcal{F}(T_{n+1}, T_n, U_n^k) + \mathcal{G}(T_{n+1}, T_n, U_n^k) \\
&= \mathcal{F}(T_{n+1}, T_n, U_n) - \mathcal{G}(T_{n+1}, T_n, U_n) \\
&\quad - (\mathcal{F}(T_{n+1}, T_n, U_n^k) - \mathcal{G}(T_{n+1}, T_n, U_n^k)) \\
&\quad + \mathcal{G}(T_{n+1}, T_n, U_n) - \mathcal{G}(T_{n+1}, T_n, U_n^{k+1}) \\
&= (c_2(U_n)\Delta T^2 + c_3(U_n)\Delta T^3 + \dots) - (c_2(U_n^k)\Delta T^2 + c_3(U_n^k)\Delta T^3 + \dots) \\
&\quad + \mathcal{G}(T_{n+1}, T_n, U_n) - \mathcal{G}(T_{n+1}, T_n, U_n^{k+1}),
\end{aligned} \tag{3.13}$$

where in the third equality we use the Lemma 3.14. As $c_j, j \geq 2$ are continuously differentiable function we have

$$\begin{aligned}
&\| (c_2(U_n)\Delta T^2 + c_3(U_n)\Delta T^3 + \dots) - (c_2(U_n^k)\Delta T^2 + c_3(U_n^k)\Delta T^3 + \dots) \| \\
&\leq \Delta T^2 \| c_2(U_n) - c_2(U_n^k) \| + \Delta T^3 \| c_3(U_n) - c_3(U_n^k) \| + \dots \\
&\leq C_2 \Delta T^2 \| U_n - U_n^k \| + C_3 \Delta T^3 \| U_n - U_n^k \| + \dots = C_1 \Delta T^2 \| U_n - U_n^k \|.
\end{aligned} \tag{3.14}$$

Taking norm in (3.13) and using (3.14) and the Lipschitz condition given in Lemma 3.13 we have the following recurrence relation for the error $E_{n+1}^{k+1} = U(T_{n+1}) - U_{n+1}^{k+1}$ as

$$\| E_{n+1}^{k+1} \| \leq C_1 \Delta T^2 \| E_n^k \| + \| P_1 \| \| E_n^{k+1} \|. \tag{3.15}$$

The recurrence relation in (3.15) can be written in the following matrix form

$$e^{k+1} = C_1 \Delta T^2 \mathbb{T}(\beta) e^k, \tag{3.16}$$

where $e^k = [\| E_1^k \|, \| E_2^k \|, \dots, \| E_N^k \|]^t$, and $\beta = \| P_1 \|$. Clearly the iteration matrix in (3.16) is Nilpotent, hence we have finite step convergence. Now to get the stated result we use the Lemma 3.4 and infinity norm in (3.16). \square

Next we discuss the stability and convergence behaviour of the Parareal algorithm NPA-II. In this case both fine and coarse propagators are nonlinear. To get the coarse operator in its explicit form we use Newton method to the nonlinear system. So the solution of the nonlinear coarse operator in (2.3) is the zeros of the following nonlinear equations

$$H(Y) = Y + \epsilon^2 \Delta t D_h^2 Y - \Delta t D_h Y^3 - \hat{Y}, \tag{3.17}$$

where $Y = U^{n+1} \in \mathbb{R}^{N_x-2}$ and $\hat{Y} = (I - \Delta t D_h)U^n \in \mathbb{R}^{N_x-2}$. After applying the Newton method on (3.17) with iteration index m and then simplifying we have

$$Y_{m+1} = (I + \epsilon^2 \Delta t D_h^2 - 3\Delta t D_h \text{diag}(Y_m^2))^{-1}(\hat{Y} - 2\Delta t D_h \text{diag}(Y_m^2)Y_m). \tag{3.18}$$

Numerical experiments suggest that upon convergence of the Newton Method the term $\text{diag}(Y_m^2) \approx I$ away from interface region of width ϵ , similar behaviour also observed in [3]. If one uses initial solution as an initial guess for the Newton method then the coarse operator (2.3) takes the following form

$$\mathcal{G}(T_{n+1}, T_n, U) = [(I + \Delta t D_h^2 - 3\Delta t D_h)^{-1}(I - 3\Delta t D_h)]^m U, \tag{3.19}$$

for some Newton iteration m . Next we prove some auxiliary results.

Lemma 3.17 (Growth of Coarse Operator in NPA-II). *The coarse operator in (3.19) satisfies the growth condition $\|\mathcal{G}(T_{n+1}, T_n, U)\| \leq \|U\|, \forall U \in \mathbb{R}^{N_x-2}$.*

Proof. We have $\|\mathcal{G}(T_{n+1}, T_n, U)\| \leq \|P_3\|^m \|U\|$. Now $\|P_3\| < 1$ follows from Lemma 3.1, hence the result. \square

Lemma 3.18 (Lipschitz of \mathcal{G} in NPA-II). *The coarse operator in (3.19) satisfies the Lipschitz condition $\|\mathcal{G}(T_{n+1}, T_n, U_1) - \mathcal{G}(T_{n+1}, T_n, U_2)\| \leq \|P_3\| \|U_1 - U_2\|, \forall U_1, U_2 \in \mathbb{R}^{N_x-2}$.*

Proof. The result is straight forward. \square

Lemma 3.19 (LTE Differences in NPA-II). *Let $\mathcal{F}(T_{n+1}, T_n, U)$ and $\mathcal{G}(T_{n+1}, T_n, U)$ be the fine and coarse operator generated by the nonlinear scheme in (2.3), then the following LTE differences hold*

$$\mathcal{F}(T_{n+1}, T_n, U) - \mathcal{G}(T_{n+1}, T_n, U) = c_2(U)\Delta T^2 + c_3(U)\Delta T^3 + \dots,$$

where $c_j(U)$ are continuously differentiable function for $j = 2, 3, \dots$

Proof. The result follows from the Lemma 3.14. \square

Theorem 3.20 (Stability of NPA-II). *The algorithm NPA-II is stable, i.e., for each n and k , $\|U_{n+1}^{k+1}\| \leq \|u^0\| + C(n+1)\Delta T^2 \left(\max_{0 \leq j \leq n} \|U_j^k\| \right)$, for some constant C .*

Proof. The proof can be obtained by following the proof of Theorem 3.15. \square

Theorem 3.21 (Convergence of NPA-II). *If the propagator \mathcal{F} and \mathcal{G} in (2.3) satisfy LTE differences given in Lemma 3.19 and \mathcal{G} satisfies the Lipschitz condition given in Lemma 3.18, then the algorithm NPA-II satisfies the following error estimate*

$$\max_{1 \leq j \leq N} \|E_j^{k+1}\| \leq (C_2 \Delta T^2)^{k+1} \min \left\{ \left(\frac{1 - \beta^{N-1}}{1 - \beta} \right)^{k+1}, \binom{N-1}{k+1} \right\} \max_{1 \leq j \leq N} \|E_j^0\|,$$

where $\beta = \|P_3\|$, and C_2 is a constant related to LTE.

Proof. The proof is similar to the proof of Theorem 3.16. \square

Remark 3.22. (1) One can obtain the convergence estimate of NPA-II at the semi-discrete level by estimating coarse operator at the semi-discrete level. (2) Explicit expression of the linear and nonlinear Parareal algorithms in 2D or 3D can be achieved by extending the 1D case naturally. (3) Convergence proof of Parareal method in higher dimension follows from the 1D case by deriving the discrete Laplacian D_h for regular or irregular computational domain. (4) The term $\binom{N-1}{k+1} = \frac{1}{(k+1)!} \prod_{j=0}^{k-1} (N-j)$ which appears in all of the convergence results says that methods converges at most $N+1$ iteration. So we always have finite step convergence to the fine solution.

4. NUMERICAL ILLUSTRATION

In this section we present the numerical experiments for the linear and non-linear Parareal algorithms, which are analyzed in this article. The Parareal iterations start with an initial guess given by coarse operator and stop as the error measured in $\| U - U^k \|_{L^\infty(0,T;L^2(\Omega))}$ reaches a tolerance of 10^{-6} , where U is the discrete fine solution and U^k is the discrete Parareal solution at k -th iteration. We consider the spatial domain $\Omega = (0, 1)$ in 1D and $\Omega = (0, 1)^2$ in 2D.

4.1. Numerical Experiments of PA-I. We first discuss the numerical experiments in 1D. We run the PA-I algorithm with fixed parameters $T = 1, h = 1/64, N = 20, J = 200$ and two different $\epsilon = 0.0725, 0.725$. The comparison of theoretical error estimate from Theorem 3.7 and numerical error reduction can be seen in Figure 1. We observe that for larger ϵ the theoretical bound given in Theorem 3.7 is much sharper than the bound corresponding to smaller ϵ . The reason being is that even though $\alpha < 1$ & $\beta < 1$ in Theorem 3.7 for every choice of ϵ , the values of α, β increases to one as ϵ decreases. Now we study the convergence behaviour of

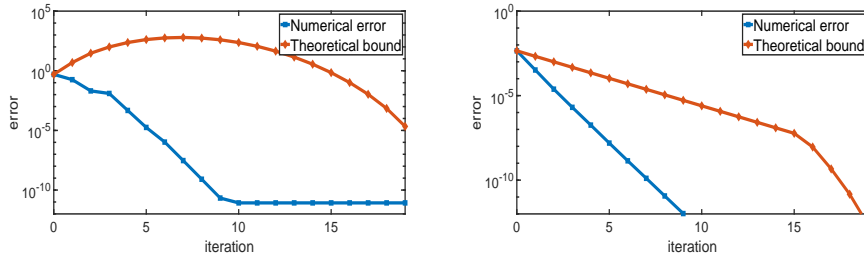


FIGURE 1. PA-I: Comparison of theoretical and numerical error.
On the left $\epsilon = 0.0725$, and on the right $\epsilon = 0.725$.

PA-I on the choice of ΔT . In Figure 2 we plot the error curves for different ΔT with fixed parameters $\epsilon = 0.0725, h = 1/64, J = 200$ on the left panel and we can see that the method works well for large ΔT . On the right in Figure 2 we plot the error curves for different mesh sizes with $T = 1, \epsilon = 0.0725, h = 1/64, \Delta t = 1/200$. We observe that convergence is independent of mesh parameters. We plot the error

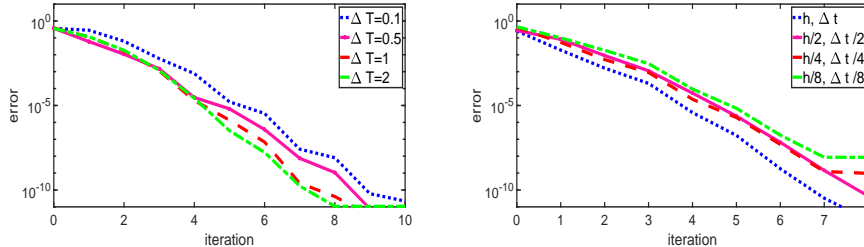


FIGURE 2. PA-I: On the left convergence for different ΔT ; On the right convergence for different $h, \Delta t$.

curves on the left panel in Figure 3 for short as well as long time window with

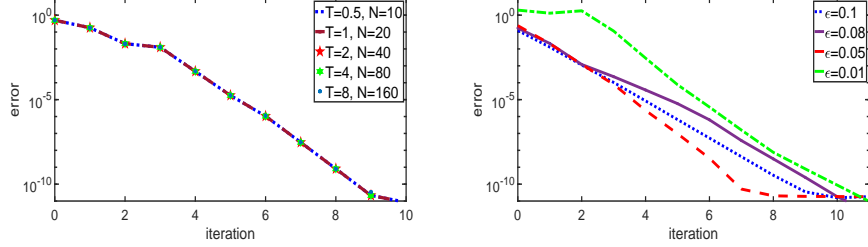


FIGURE 3. PA-I: On the left convergence for different T, N , and on the right convergence for different ϵ .

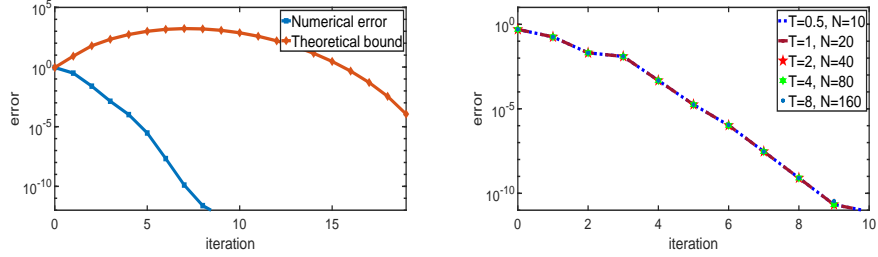


FIGURE 4. PA-I: On the left comparison of theoretical and numerical error, and on the right convergence for different T, N .

$\epsilon = 0.0725, J = 200$ and $h = 1/64$. The method converges in four iterations to the fine solution of temporal accuracy $O(10^{-4})$ for different T . By ignoring the computational cost of the coarse operator, we can see that the Parareal method is 40 times faster than serial method on a single processor for $T = 8$. It is evident from the left plot of Figure 3 that one can achieve more speed up by including more processors (N). To see the dependency on the parameter ϵ , we plot the error curves on the right panel in Figure 3 for different ϵ by taking $T = 1, N = 50, J = 200$. We observe that the method is almost immune to the choice of ϵ .

To perform the numerical experiments in 2D we take the discretization parameter $h = 1/32$ on both direction. We plot the comparison of error contraction on the left panel in Figure 4 for $T = 1, N = 20, J = 200$ and $\epsilon = 0.0725$. We plot the error curves on the right in Figure 4 for short as well as long time window with $\epsilon = 0.0725, J = 200$. The method converges in four iterations to the fine solution of temporal accuracy $O(10^{-4})$ for different T . We observe similar convergence behaviour of PA-I in 2D as in 1D with respect to different situation and so we skip those experiments here.

4.2. Numerical Experiments of PA-II. 1D case: The comparison of numerical error and theoretical estimate from Theorem 3.9 can be seen from the left plot in Figure 5 for $T = 1, h = 1/64, N = 20, J = 200$ and $\epsilon = 0.0725$. On the right we plot the error curves for more refined solution for $T = 1, \epsilon = 0.0725, h = 1/64, \Delta t = 1/200$. We can see that the convergence is independent of mesh parameters. We plot the error curves on the left in Figure 6 for short as well as long time window with $\epsilon = 0.0725, J = 200$ and $h = 1/64$. We can see that one get the speed up compared

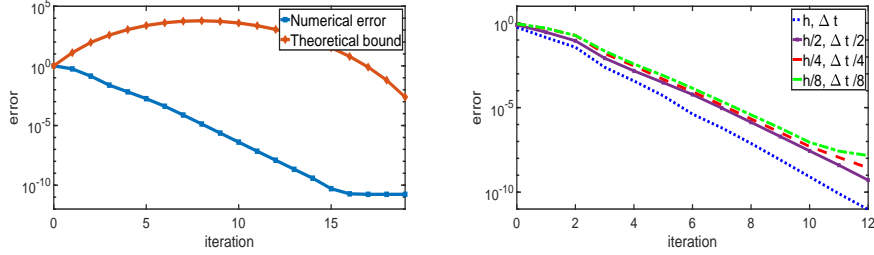


FIGURE 5. PA-II: On the left comparison of theoretical and numerical error, and on the right convergence for different mesh sizes.

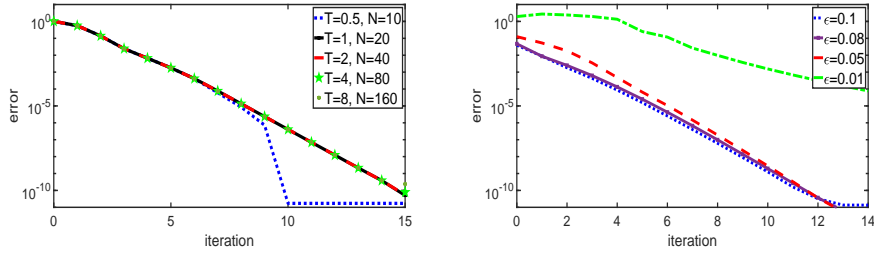


FIGURE 6. PA-II: On the left convergence for different T, N , and on the right ϵ dependency on the convergence.

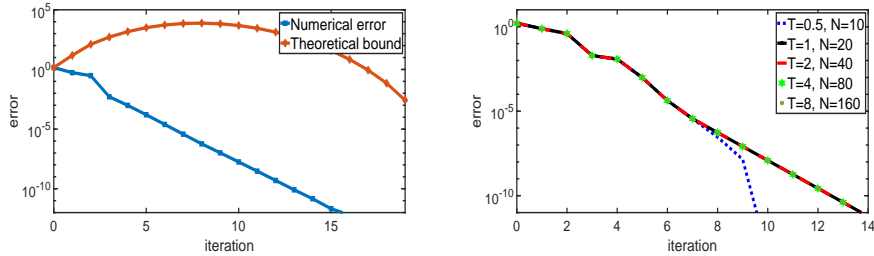


FIGURE 7. PA-II: On the left comparison of theoretical and numerical error, and on the right convergence for different T, N .

to serial solve. To see the dependency on the parameter ϵ , we plot the error curves on the right in Figure 6 for different ϵ by taking $T = 1, N = 50, J = 200$. We can see that the PA-II is sensitive to the choice of ϵ , namely for the very small ϵ .

2D case: We take the same discretization parameter $h = 1/32$ on both direction. We plot the comparison of error contraction on the left panel in Figure 7 for $T = 1, N = 20, J = 200$ and $\epsilon = 0.0825$. We plot the error curves on the right in Figure 7 for short as well as long time window with $\epsilon = 0.0725, J = 200$. We observe similar convergence behaviour of PA-II in 2D as in 1D with respect to different situation.

4.3. Numerical Experiments of PA-III. **1D case:** The comparison of numerical error and theoretical estimates from Theorem 3.11 can be seen in the left plot of

Figure 8 for $T = 1, h = 1/64, N = 20, J = 200$ and $\epsilon = 0.0725$. On the right panel we plot the error curves for more refined solution for $T = 1, \epsilon = 0.0725, h = 1/64, \Delta t = 1/200$. We can see that convergence is independent of mesh parameters. We plot the error curves on the left in Figure 9 for short as well as long time

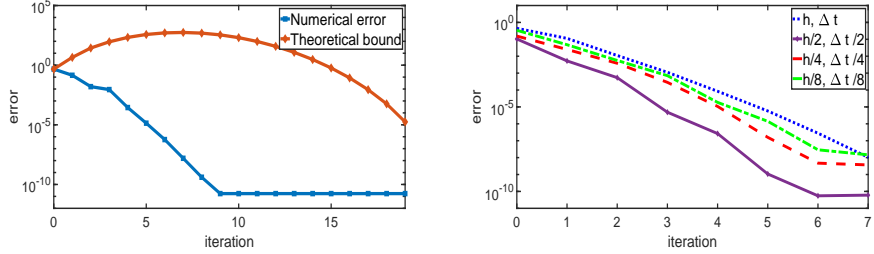


FIGURE 8. PA-III: On the left comparison of theoretical and numerical error, and on the right convergence for different mesh sizes.

window with $\epsilon = 0.0725, J = 200$ and $h = 1/64$. The method converges in four iteration to the fine resolution of temporal accuracy $O(10^{-4})$ for different T and one get the speed up compared to sequential solve. To see the dependency on the parameter ϵ , we plot the error curves on the right in Figure 9 for different ϵ by taking $T = 1, N = 50, J = 200$. We can see that the convergence of PA-III is independent of the choice of ϵ . As PA-II and PA-III converge to the fine solution given by (2.5), we can compare them. Since PA-II is sensitive towards small ϵ , therefore PA-III is the best choice to approximate fine solution given by (2.5).

2D case: We take the discretization parameter $h = 1/32$ on both direction and plot the comparison of error contraction on the left in Figure 10 for $T = 1, N = 20, J = 200$ and $\epsilon = 0.0625$. We plot the error curves on the right for short as well as long time window with $\epsilon = 0.0725, J = 200$. We observe similar convergence behaviour of PA-III in 2D as in 1D for different situation.

4.4. Numerical Experiments of NPA-I. 1D case: The nonlinear fine propagator is obtained using the Newton method with a tolerance $1e-10$. To implement the theoretical bound prescribed in Theorem 3.16 we have to estimate the quantity C_1 numerically, which depends on choice of $\epsilon, J, \Delta T, u^0$. The comparison of numerical error and theoretical estimates can be seen on the left plot of Figure

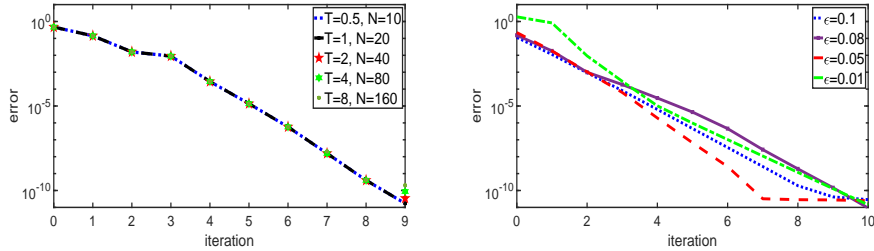


FIGURE 9. PA-III: On the left convergence for different T, N , and on the right ϵ dependency on the convergence.

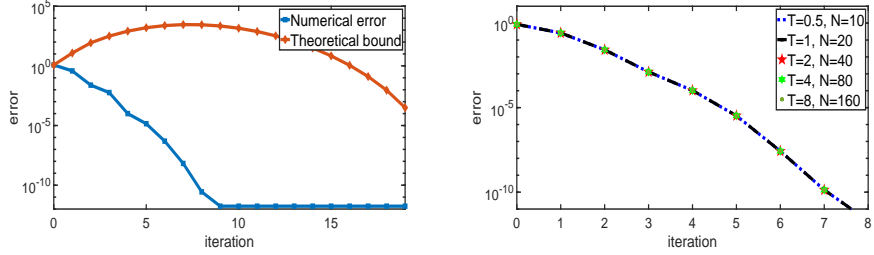


FIGURE 10. PA-III: On the left comparison of theoretical and numerical error, and on the right convergence for different T, N .

11 for $\Delta T = 1, h = 1/64, N = 20, J = 200, \epsilon = 0.0725$ and $C_1 = 0.1181$. On the right panel in Figure 11 we plot the error curves for more refined solution for $T = 1, \epsilon = 0.0725, h = 1/64, \Delta t = 1/200$. We can see that convergence is independent of mesh parameters. We plot the error curves on the left in Figure 12

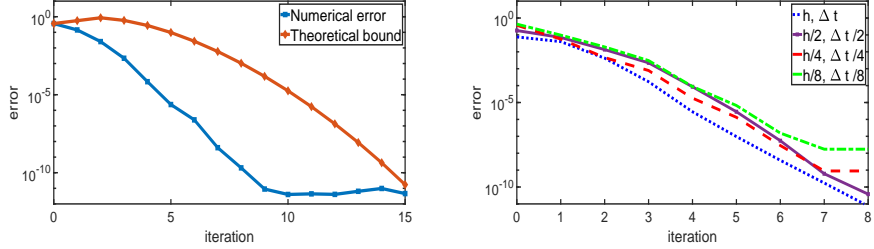


FIGURE 11. NPA-I: On the left comparison of theoretical and numerical error, and on the right convergence of refined solution.

for short as well as long time window with $\epsilon = 0.0725, J = 200$ and $h = 1/64$. To see the dependency on the parameter ϵ , we plot the error curves on the right panel in Figure 12 for different ϵ by taking $T = 1, N = 50, J = 200$. We can see that the NPA-I is independent of the choice of ϵ . On the left panel in Figure 13 we plot the error curves with respect to different number of time slices for $T = 50, \epsilon = 0.0725, h = 1/64, J = 150$. We can see that convergence is independent

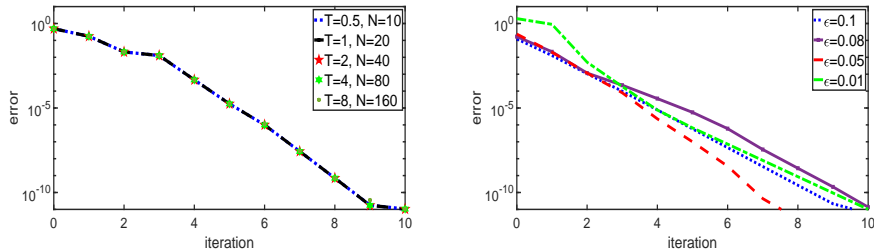


FIGURE 12. NPA-I: On the left convergence for different T, N , and on the right ϵ dependency on convergence.

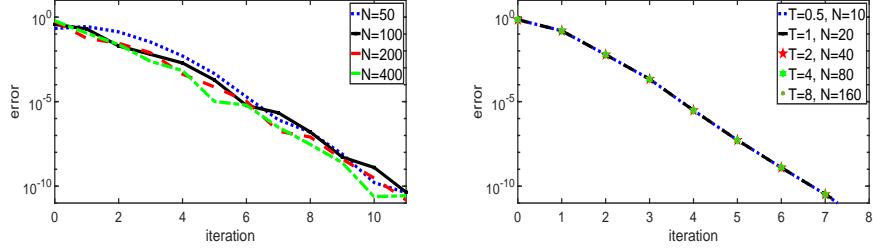


FIGURE 13. NPA-I: On the left convergence for different N , and on the right convergence for different T, N in 2D.

of time decomposition. One can observe that a speed up of 80 times compared to serial solve for $N = 400$.

2D case: We take the discretization parameter $h = 1/32$ on both direction. As we observe similar convergence behaviour in 2D as in 1D, we only plot the error curves on the right in Figure 13 for short as well as long time window with $\epsilon = 0.0725, J = 200$. We omit the other experiments in 2D as we observe similar convergence behaviour as in 1D.

4.5. Numerical Experiments of NPA-II. 1D case: In this case we have nonlinear solvers for both fine and coarse propagator by the Newton method with a tolerance $1e-10$. To implement the theoretical bound prescribed in Theorem 3.21 we have to estimate the quantity C_1 numerically, which depends on the choice of $\epsilon, J, \Delta T, u^0$. The comparison of numerical error and theoretical estimate can be seen on the left plot of Figure 14 for $\Delta T = 1, h = 1/64, N = 20, J = 200, \epsilon = 0.0725$ and $C_1 = 0.1498$. On the right we plot the error curves for more refined solution for $T = 1, \epsilon = 0.0725, h = 1/64, \Delta t = 1/200$. We can see that convergence is independent of mesh parameters. We plot the error curves on the left in Figure 15

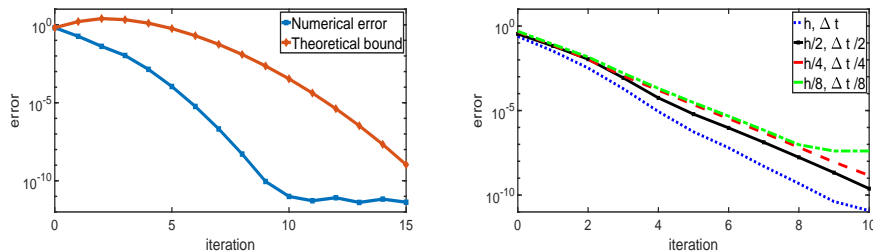


FIGURE 14. NPA-II: On the left comparison of theoretical and numerical error, and on the right convergence of refined solution.

for short as well as long time window with $\epsilon = 0.0725, J = 150$ and $h = 1/64$. To see the dependency on the parameter ϵ , we plot the error curves on the right in Figure 15 for different ϵ by taking $T = 1, N = 50, J = 200$. We can see that the NPA-II is independent of the choice of ϵ . At this point we can compare NPA-I and NPA-II as both have the fine solution given by (2.3). Between these two, NPA-II is expansive because of the nonlinear coarse solver and we take almost same number

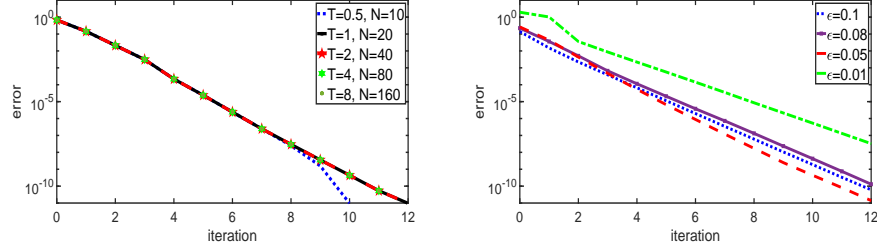


FIGURE 15. NPA-II: On the left convergence for different T, N , and on the right ϵ dependency on convergence.

iteration to converge as in the case of NPA-I. Therefore it is better to use NPA-I while computing the nonlinear approximation of the CH equation. We skip the numerical experiments in 2D as we observe similar behaviour as in 1D.

4.6. Numerical Experiments of Neumann-Neumann method as fine solver in PA-I. In all of the above experiments we use the scheme (2.3), (2.4) or (2.5) as fine solver. In practise one try to solve the CH equation in much larger domain with very fine mesh, that results in a very large scale algebraic system (as the spatial dimension increases). In this context one introduce parallelism in space by using Domain Decomposition (DD) based techniques, here we use a non-overlapping DD method, namely Neumann-Neumann (NN) method. The NN method for the CH equation in space is considered in [17] for two subdomain decomposition and in [18] for multiple subdomain decomposition, where they use (2.3) and (2.4) to build linear and nonlinear NN solver. Here we use linear NN method as fine solver in the PA-I algorithm. In every subinterval $[T_{n-1}, T_n]$ we compute the solution as the following:

Let $\Omega \subset \mathbb{R}$ is decomposed into non-overlapping subdomains $\{\Omega_i, 1 \leq i \leq N_0\}$. So to solve (2.4) at each time level the NN method starts with initial guesses $g_i^{[0]}, h_i^{[0]}$ along the interfaces $\Gamma_i = \partial\Omega_i \cap \partial\Omega_{i+1}$ for $i = 1, \dots, N_0 - 1$, and then it's a two step execution: at each iteration ν , one first solves Dirichlet sub-problems on each Ω_i in parallel, and then compute the jump in Neumann traces on the interfaces and one solves the Neumann subproblems on each Ω_i in parallel,

$$\left\{ \begin{array}{l} \begin{bmatrix} I & -\delta_t \Delta \\ \epsilon^2 \Delta - c^2 & I \end{bmatrix} \begin{bmatrix} u_i^{[\nu]} \\ v_i^{[\nu]} \end{bmatrix} = \begin{bmatrix} f_u \\ f_v \end{bmatrix}, \quad \text{in } \Omega_i, \\ \begin{bmatrix} u_i^{[\nu]} \\ v_i^{[\nu]} \end{bmatrix} = 0, \quad \text{on } \partial\Omega_i \cap \partial\Omega, \\ \begin{bmatrix} u_i^{[\nu]} \\ v_i^{[\nu]} \end{bmatrix} = \begin{bmatrix} g_{i-1}^{[\nu-1]} \\ h_{i-1}^{[\nu-1]} \end{bmatrix} \quad \text{on } \Gamma_{i-1}, \\ \begin{bmatrix} u_i^{[\nu]} \\ v_i^{[\nu]} \end{bmatrix} = \begin{bmatrix} g_i^{[\nu-1]} \\ h_i^{[\nu-1]} \end{bmatrix} \quad \text{on } \Gamma_i, \end{array} \right. \quad (4.1)$$

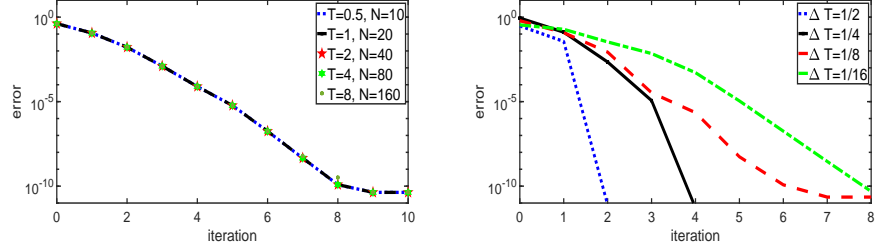


FIGURE 16. On the left: different T, N , and on the right: different ΔT .

$$\left\{ \begin{array}{l} \begin{bmatrix} I & -\delta_t \Delta \\ \epsilon^2 \Delta - c^2 & I \end{bmatrix} \begin{bmatrix} \phi_i^{[\nu]} \\ \psi_i^{[\nu]} \end{bmatrix} = 0, \quad \text{in } \Omega_i, \\ \begin{bmatrix} \phi_i^{[\nu]} \\ \psi_i^{[\nu]} \end{bmatrix} = 0, \quad \text{on } \partial\Omega_i \cap \partial\Omega, \\ \frac{\partial}{\partial x} \begin{bmatrix} \phi_i^{[\nu]} \\ \psi_i^{[\nu]} \end{bmatrix} = \frac{\partial}{\partial x} \begin{bmatrix} u_{i-1}^{[\nu]} - u_i^{[\nu]} \\ v_{i-1}^{[\nu]} - v_i^{[\nu]} \end{bmatrix}, \quad \text{on } \Gamma_{i-1} \\ \frac{\partial}{\partial x} \begin{bmatrix} \phi_i^{[\nu]} \\ \psi_i^{[\nu]} \end{bmatrix} = \frac{\partial}{\partial x} \begin{bmatrix} u_i^{[\nu]} - u_{i+1}^{[\nu]} \\ v_i^{[\nu]} - v_{i+1}^{[\nu]} \end{bmatrix}, \quad \text{on } \Gamma_i, \end{array} \right. \quad (4.2)$$

except for the first and last subdomains, where at the physical boundaries the Dirichlet condition in the Dirichlet step and Neumann condition in the Neumann step are replaced by homogeneous Dirichlet condition. Then the interface traces are updated by

$$\begin{bmatrix} g_i^{[\nu]} \\ h_i^{[\nu]} \end{bmatrix} = \begin{bmatrix} g_i^{[\nu-1]} \\ h_i^{[\nu-1]} \end{bmatrix} - \theta \left[\begin{bmatrix} \phi_i^{[\nu]} - \phi_{i+1}^{[\nu]} \\ \psi_i^{[\nu]} - \psi_{i+1}^{[\nu]} \end{bmatrix} \right]_{|\Gamma_i},$$

where $\theta \in (0, 1)$ is a relaxation parameter. In NN method (4.1)-(4.2), $\delta_t = \Delta t$ is the fine time step, $f_u = u^n$, $f_v = -u^n$, $c = (u^n)^2$, where u^n is solution of the CH equation at n -th time step. In a similar fashion one can formulate NN method for the scheme given in (2.5) and use in PA-III as a fine solver. There is also a nonlinear version of (4.1) in [18], which can be used as a fine solver in the nonlinear Parareal case. To see the numerical experiments in 1D, we take $N_0 = 8$ (equal subdomain), $\theta = 1/4$. Note that the parareal solution converges towards fine solution given by the NN method. For convergence of NN method at each time level we set the tolerance as $\| g_i^{[\nu+1]} - g_i^{[\nu]} \|_{L^2} \leq 10^{-10}$ and $\| h_i^{[\nu+1]} - h_i^{[\nu]} \|_{L^2} \leq 10^{-10}$. The convergence of NN method described in [18]; here we study the convergence of Parareal method PA-I to the NN solution given by (4.1). We plot the error curves on the left in Figure 16 for short as well as long time window with $\epsilon = 0.0725$, $J = 200$ and $h = 1/128$. The left plot in Figure 16 is almost identical to the left plot given in Figure 3. So we have similar convergence behaviour for NN method as fine solver with an advantage of more parallelism in the system. To see the dependency on the parameter ΔT , we plot the error curves on the right in Figure 16 for different ΔT by taking $T = 1$, $J = 150$, $\epsilon = 0.0725$. We can observe that convergence is robust.

5. CONCLUSIONS

We propose and studied the linear and nonlinear Parareal algorithms for the CH equation. We showed convergence of all the proposed Parareal algorithms. Numerical experiments show that proposed methods are very robust and one obtains a reasonable speed up by introducing more processor.

ACKNOWLEDGEMENT

The authors would like to thank the CSIR (File No:09/1059(0019)/2018-EMR-I) and DST-SERB (File No: SRG/2019/002164) for the research grant and IIT Bhubaneswar for providing excellent research environment.

REFERENCES

- [1] L. BAFFICO, S. BERNARD, Y. MADAY, G. TURINICI, AND G. ZÉRAH, *Parallel-in-time molecular-dynamics simulations*, Physical Review E, 66 (2002), p. 057701.
- [2] A. L. BERTOZZI, S. ESEDOĞLU, AND A. GILLETTE, *Inpainting of binary images using the Cahn-Hilliard equation*, IEEE Trans. Image Process., 16 (2007), pp. 285–291.
- [3] S. C. BRENNER, A. E. DIEGEL, AND L.-Y. SUNG, *A robust solver for a mixed finite element method for the cahn-hilliard equation*, Journal of Scientific Computing, 77 (2018), pp. 1234–1249.
- [4] J. W. CAHN, *On spinodal decomposition*, Acta Metall, 9 (1961), pp. 795–801.
- [5] J. W. CAHN AND W. HILLIARD, *Free energy of a nonuniform system. i. interfacial free energy*, J. Chem. Phys., 28 (1958), pp. 258–267.
- [6] D. S. COHEN AND J. D. MURRAY, *A generalized diffusion model for growth and dispersal in a population*, Journal of Mathematical Biology, 12 (1981), pp. 237–249.
- [7] Q. DU AND R. A. NICOLAIDES, *Numerical analysis of a continuum model of phase transition*, SIAM J. Numer. Anal., 28 (1991), pp. 1310–1322.
- [8] C. M. ELLIOTT AND D. A. FRENCH, *Numerical studies of the cahn-hilliard equation for phase separation*, IMA Journal of Applied Mathematics, 38 (1987), pp. 97–128.
- [9] C. M. ELLIOTT AND Z. SONGMU, *On the Cahn-Hilliard equation*, Arch. Rational Mech. Anal., 96 (1986), pp. 339–357.
- [10] D. J. EYRE, *Unconditionally gradient stable time marching the Cahn-Hilliard equation*, in Computational and mathematical models of microstructural evolution (San Francisco, CA, 1998), vol. 529 of Mater. Res. Soc. Symp. Proc., MRS, Warrendale, PA, 1998, pp. 39–46.
- [11] ———, *An unconditionally stable one-step scheme for gradient systems*, Unpublished article, (1998).
- [12] C. FARHAT AND M. CHANDESRIS, *Time-decomposed parallel time-integrators: theory and feasibility studies for fluid, structure, and fluid-structure applications*, International Journal for Numerical Methods in Engineering, 58 (2003), pp. 1397–1434.
- [13] P. F. FISCHER, F. HECHT, AND Y. MADAY, *A parareal in time semi-implicit approximation of the navier-stokes equations*, in Domain decomposition methods in science and engineering, Springer, 2005, pp. 433–440.
- [14] D. FURIHATA, *A stable and conservative finite difference scheme for the cahn-hilliard equation*, Numerische Mathematik, 87 (2001), pp. 675–699.
- [15] M. J. GANDER, *50 years of time parallel time integration*, in Multiple shooting and time domain decomposition methods, Springer, 2015, pp. 69–113.
- [16] M. J. GANDER AND S. VANDEWALLE, *Analysis of the parareal time-parallel time-integration method*, SIAM Journal on Scientific Computing, 29 (2007), pp. 556–578.
- [17] G. GARAI, *Convergence of the neumann-neumann method for the cahn-hilliard equation*, arXiv preprint arXiv:2107.03812, (2021).
- [18] G. GARAI AND B. C. MANDAL, *Convergence of linear and nonlinear substructuring methods for the cahn-hilliard equation*, 2021.
- [19] Y.-T. KIM, N. PROVATAS, N. GOLDENFELD, AND J. DANTZIG, *Universal dynamics of phase-field models for dendritic growth*, Physical Review E, 59 (1999), p. R2546.

- [20] D. LEE, J.-Y. HUH, D. JEONG, J. SHIN, A. YUN, AND J. KIM, *Physical, mathematical, and numerical derivations of the cahn–hilliard equation*, Computational Materials Science, 81 (2014), pp. 216–225.
- [21] J.-L. LIONS, Y. MADAY, AND G. TURINICI, *A “parareal” in time discretization of pde’s*, Comptes Rendus De L Academie Des Sciences Serie I-Mathematique, 332 (2001), pp. 661–668.
- [22] S. LIU, F. WANG, AND H. ZHAO, *Global existence and asymptotics of solutions of the cahn–hilliard equation*, Journal of Differential Equations, 238 (2007), pp. 426–469.
- [23] J. SHEN, J. XU, AND J. YANG, *The scalar auxiliary variable (sav) approach for gradient flows*, Journal of Computational Physics, 353 (2018), pp. 407–416.
- [24] J. SHIN, D. JEONG, AND J. KIM, *A conservative numerical method for the cahn–hilliard equation in complex domains*, Journal of Computational Physics, 230 (2011), pp. 7441–7455.
- [25] S. TREMAINE, *On the origin of irregular structure in saturn’s rings*, The Astronomical Journal, 125 (2003), p. 894.
- [26] B. P. VOLLMAYR-LEE AND A. D. RUTENBERG, *Fast and accurate coarsening simulation with an unconditionally stable time step*, Physical Review E, 68 (2003), p. 066703.
- [27] S. M. WISE, J. S. LOWENGRUB, AND V. CRISTINI, *An adaptive multigrid algorithm for simulating solid tumor growth using mixture models*, Math. Comput. Modelling, 53 (2011), pp. 1–20.
- [28] X. YANG, *Linear, first and second-order, unconditionally energy stable numerical schemes for the phase field model of homopolymer blends*, Journal of Computational Physics, 327 (2016), pp. 294–316.
- [29] X. YANG, J. ZHAO, Q. WANG, AND J. SHEN, *Numerical approximations for a three-component cahn–hilliard phase-field model based on the invariant energy quadratization method*, Mathematical Models and Methods in Applied Sciences, 27 (2017), pp. 1993–2030.

GOBINDA GARAI

SCHOOL OF BASIC SCIENCES, INDIAN INSTITUTE OF TECHNOLOGY BHUBANESWAR, INDIA

Email address: gg14@iitbbs.ac.in

BANKIM C. MANDAL

SCHOOL OF BASIC SCIENCES, INDIAN INSTITUTE OF TECHNOLOGY BHUBANESWAR, INDIA

Email address: bmandal@iitbbs.ac.in

